



# Ultrafast lithium storage of high dispersed silicon and titanium oxide nanoparticles in carbon



Geon-Hyoung An <sup>a</sup>, **Hyo-Jin Ahn** <sup>a, b, \*</sup>

<sup>a</sup> Program of Materials Science & Engineering, Convergence Institute of Biomedical Engineering and Biomaterials, Seoul National University of Science and Technology, Seoul 139-743, South Korea

<sup>b</sup> Department of Materials Science and Engineering, Seoul National University of Science and Technology, Seoul 139-743, South Korea

## ARTICLE INFO

### Article history:

Received 19 January 2017

Received in revised form

8 March 2017

Accepted 22 March 2017

Available online 23 March 2017

### Keywords:

Li-ion battery

Anode

Silicon nanoparticles

Titanium oxide nanoparticles

Dispersion

Composites

## ABSTRACT

Silicon and carbon composites as an anode material in lithium-ion batteries are the most promising candidates to replace conventional graphite, owing to their synergetic effects of high capacity and excellent mechanical stability. Despite these appealing merits, the significant challenge is directly related to the poor dispersion of Si nanoparticles in the carbon nanofiber (CNF) matrix, leading to a structural collapse after cycling due to the large volume change (~300%) of Si. Thus, we synthesized unique composites of high-dispersed Si and titanium oxide (TiO<sub>2</sub>) nanoparticles in the CNF matrix (Si/TiO<sub>2</sub>/CNF) using the complexation of TiO<sub>2</sub> nanoparticles in order to the high-dispersed Si nanoparticles. The Si/TiO<sub>2</sub>/CNF electrode presents enhanced electrochemical properties including excellent cycling stability and high specific capacity (947 mA h g<sup>-1</sup> at 100 mA g<sup>-1</sup> after 100 cycles), remarkable high-rate performance (612 mA h g<sup>-1</sup> at 2000 mA g<sup>-1</sup>), and outstanding ultrafast cycling stability (478 mA h g<sup>-1</sup> at 2000 mA g<sup>-1</sup> after 100 cycles). It is revealed that the high-dispersed Si nanoparticles can maintain the initial structure after cycling, which definitely demonstrates the superiority of our concept.

© 2017 Elsevier B.V. All rights reserved.

## 1. Introduction

Lithium-ion batteries (LIBs) have been acknowledged as the principal power source for portable electronic devices, such as smartphones, mobile watches, and laptops, owing to their notable performance characteristics such as high energy density, good cycling stability, environmental friendliness, low self-discharge rate, and lack of memory effects [1–5]. Nevertheless, the LIB technologies for utilization in fully electric vehicles (EVs) are still lacking, because of the short driving distance of 150–200 miles, implying the relatively low energy density of LIBs [5,6]. To solve the above-mentioned problem, the LIB performances are constantly improved by advanced anode electrode materials. It is well known that graphite, with a low theoretical capacity of 372 mA h g<sup>-1</sup>, was commercially used for the anode material in LIBs, which has partly limited the energy density of LIBs [7,8]. For this reason, the exploration of advanced anode materials such as Si, transition metal dichalcogenides, and alloy with much higher

capacities is conducted by many researchers [9–12]. Among various anode materials, Si has been mostly commonly recognized as a promising candidate, owing to its high theoretical capacity (~4200 mA h g<sup>-1</sup>) and low working voltage of <0.5 V compared to Li/Li<sup>+</sup> [13–16]. However, the structural deterioration of Si and the electrical contact loss between the electrode materials and the current collector, which results from the large volume change (~300%) of Si during the insertion/extraction of Li ions, leads to rapid capacity decay.

To circumvent this problem, many attempts have been carried out to achieve efficient composites using the carbon matrix [17–22]. The carbon matrix was generally used to perform as the physical buffer layer to alleviate the mechanical stress during the insertion/extraction of Li ions. In addition, the carbon matrix can enhance the electrical conductivity, leading to high-rate performance [17–22]. Among the various carbon matrices, the carbon nanofiber (CNF) matrix showed an enhanced electrochemical performance because of the effective accommodation of volume changes, high electrical conductivity, transport facilitation for Li ions, and flexibility [23–38]. Furthermore, various types of CNF matrix such as core–shell, porous, and hollow structures have been proved to exhibit enhanced electrochemical performance while

\* Corresponding author. Department of Materials Science and Engineering, Seoul National University of Science and Technology, Seoul 139-743, South Korea.

E-mail address: [hjahn@seoultech.ac.kr](mailto:hjahn@seoultech.ac.kr) (H.-J. Ahn).

containing Si nanoparticles. Nevertheless, the irregular dispersion of Si nanoparticles within the aggregation in the CNF matrix still presents major challenges, leading to capacity loss. In other words, the CNF matrix has not yet been efficiently used for the capsulation of Si nanoparticles. Therefore, high-dispersed Si nanoparticles in a CNF matrix are essential for the efficient accommodation of the volume change of Si nanoparticles in an LIB anode, which has not yet been studied.

Herein, we prepared high-dispersed Si and titanium dioxide (TiO<sub>2</sub>) nanoparticles in a CNF matrix; the material was fabricated by electrospinning and carbonization. In particular, the complexation of TiO<sub>2</sub> nanoparticles was introduced in the CNF matrix to improve the dispersion of Si nanoparticles. TiO<sub>2</sub> is a promising material for composites in the CNF matrix, owing to their reversible reaction with Li ions, superb cycling stability based on low volume change (~3%), environmental friendliness, and low cost [39–41]. These unique composites enable high-dispersed Si nanoparticles in the CNF matrix and allow efficient accommodation of the volume change of Si nanoparticles, increased electroactive sites, and shorter diffusion path of Li ions during cycling as the anode material for high-performance LIBs.

## 2. Experimental

### 2.1. Chemicals

Polyacrylonitrile (PAN,  $M_w = 150,000$ ) and N,N-Dimethylformamide (DMF, 99.8%) were purchased from Sigma-Aldrich. Si nanoparticles were purchased from Avention. TiO<sub>2</sub> nanoparticles (P25) were purchased from Degussa. All chemicals were used without further purification.

### 2.2. Synthesis of high-dispersed Si nanoparticles Si and TiO<sub>2</sub> nanoparticles in a CNF matrix

Synthesis of high-dispersed Si and TiO<sub>2</sub> nanoparticles in a CNF (Si/TiO<sub>2</sub>/CNF) matrix was carried out via electrospinning and carbonization. First, PAN, Si, and TiO<sub>2</sub> nanoparticles were dissolved in DMF with vigorous stirring for 12 h. For the electrospinning process, the applied voltage and feeding rate were maintained at ~13 kV and 0.03 mL h<sup>-1</sup>, respectively. The distance between the needle and the collector and was set at 15 cm under 10% relative humidity in the chamber. The as-spun nanofibers were stabilized at 200 °C for 2 h in air and then carbonized at 800 °C for 2 h under a nitrogen atmosphere. For comparison, Si nanoparticles in the CNF (Si/CNF) matrix and TiO<sub>2</sub> nanoparticles in the CNF (TiO<sub>2</sub>/CNF) matrix were prepared using the above-mentioned electrospinning and carbonization, respectively. Therefore, we synthesized three different types of composite structures: Si/CNF, TiO<sub>2</sub>/CNF, and Si/TiO<sub>2</sub>/CNF for use as the anode electrode in LIBs.

### 2.3. Characterization

The structure and morphology of the prepared sample were examined by field emission scanning electron microscopy (FESEM) and transmission electron microscopy (TEM, KBSI Gwangju center). Energy-dispersive spectrometry (EDS) was used to explore the distribution of elements. The crystal structure was observed by X-ray diffraction (XRD). The composition was investigated by thermal gravimetric analysis (TGA) in a temperature range of 200–800 °C and with a heating speed of 10 °C min<sup>-1</sup> in air.

### 2.4. Preparation of electrodes and electrochemical characterization

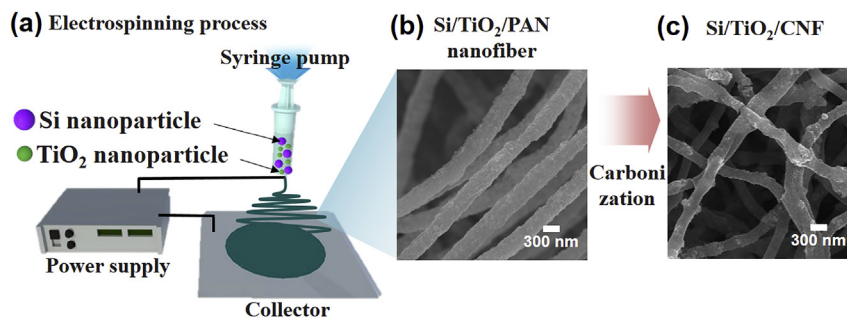
The electrochemical performance was investigated using coin-

type half cells with the prepared samples as the working electrode, Li metal as the counter electrode, 1.0 M LiPF<sub>6</sub> in ethylene carbonate-dimethyl carbonate (1:1) as electrolyte, Cu foil as the current collector, and a porous membrane as the separator. The homogenized slurry made using 80 wt% of the prepared samples, 10 wt% polyvinylidene fluoride as binder, and 10 wt% ketjenblack as conducting material in N-methyl-2-pyrrolidinone. The slurry was coated on Cu foil and then the electrode was dried at 100 °C. The mass loading of active materials was optimized and fixed with  $9.5 \pm 0.5$  mg cm<sup>-2</sup>. The coin-type half cells were assembled in a glove box filled with an argon atmosphere. The charge–discharge estimations were preformed using a cyler system (Won-A Tech, WMPG 3000) in the potential range 0.05–3.00 V (vs. Li/Li<sup>+</sup>). The cycling stability was examined for up to 100 cycles at a current density of 100 mA g<sup>-1</sup>. The high-rate performance was investigated at current densities of 100, 300, 500, 700, 1000, and 2000 mA g<sup>-1</sup>. The ultrafast cycling stability was observed up to 100 cycles at an ultrafast current density of 2000 mA g<sup>-1</sup>. The cyclic voltammetry (CV) was characterized using a potentiostat/galvanostat in the potential range 0.05–3.00 V (vs. Li/Li<sup>+</sup>), at a scan rate of 0.1 mV s<sup>-1</sup>. Electrochemical impedance spectroscopy (EIS) measurements were performed using fresh cells in the frequency range of 10<sup>5</sup> to 10<sup>-2</sup> Hz by applying an AC signal of 5 mV.

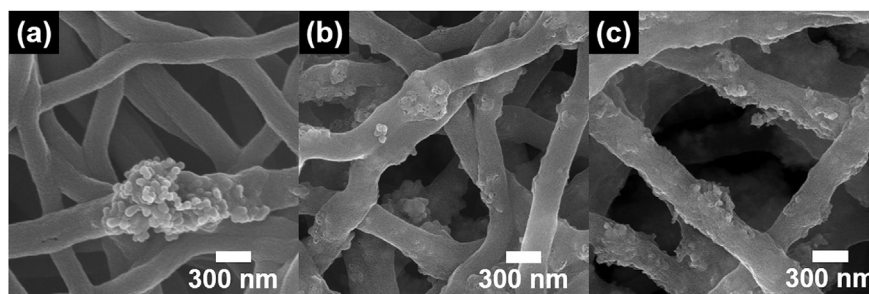
## 3. Results and discussion

Fig. 1 is an illustration of an ideal synthetic process for Si/TiO<sub>2</sub>/CNF. The electrospinning process (Fig. 1a) was set up using the electrospinning solution, power supply, syringe pump, needle, and collector. After the electrospinning process, the as-spun nanofiber composed of Si and TiO<sub>2</sub> nanoparticles in PAN nanofiber was acquired from the collector, as shown in Fig. 1b. The Si/TiO<sub>2</sub>/CNF (Fig. 1c) was successfully obtained using carbonization at 800 °C in a nitrogen atmosphere.

Fig. S1 displays FESEM and TEM images of Si (Fig. S1a and c) and TiO<sub>2</sub> (Fig. S1b and d) nanoparticles. The average sizes of Si and TiO<sub>2</sub> nanoparticles were observed in the range of 46–53 nm and 15–27 nm, respectively. Fig. 2a–c present FESEM images of Si/CNF, TiO<sub>2</sub>/CNF, and Si/TiO<sub>2</sub>/CNF. All samples showed an interconnected network structure consisting of a one-dimensional nanofiber structure. This nanofiber structure can directly provide an efficient electron transfer and a rapid Li-ion diffusion rate during cycling, which results in high-performance LIBs [42–44]. All samples possessed similar average diameters in the range of 281–303 nm. Si/CNF (Fig. 2a) exhibited smooth surfaces. In addition, the aggregation of nanoparticles in Si/CNF showed a distinct due to the low zeta potential of –71.29 mV (Fig. S2a) of Si nanoparticles in the DMF solution during the electrospinning process. The low zeta potential signifies the aggregated nanoparticles in the solution [45,46]. In other words, the aggregated Si nanoparticles in CNFs were obtained from aggregated Si nanoparticles in the DMF solution, resulting in a rapid capacity fading during cycling in LIBs. On the other hand, TiO<sub>2</sub>/CNF (Fig. 2b) showed uneven surfaces, which implies the presence of high-dispersed TiO<sub>2</sub> nanoparticles in CNFs owing to the higher zeta potential –14.35 mV (Fig. S2b) of TiO<sub>2</sub> nanoparticles in the DMF solution compared to the Si nanoparticles. Additionally, Si/TiO<sub>2</sub>/CNF (Fig. 2c) exhibited uneven surfaces, implying the presence of high-dispersed Si and TiO<sub>2</sub> nanoparticles. These FESEM results clearly indicate that the complexation of TiO<sub>2</sub> nanoparticles could assist the dispersion of Si nanoparticles in CNFs, owing to the high zeta potential –14.35 mV and small size of TiO<sub>2</sub> nanoparticles compared to Si nanoparticles. These unique composites of Si/TiO<sub>2</sub>/CNF as anode materials for LIBs can effectively relieve the volume change during insertion/extraction of Li ions, owing to the high-dispersed Si nanoparticles in the CNF matrix, leading to



**Fig. 1.** Schematic illustration of synthetic routes for Si/TiO<sub>2</sub>/CNF. (a) The electrospinning process using Si and TiO<sub>2</sub> nanoparticles in DMF solution. (b) Si/TiO<sub>2</sub>/PAN nanofiber after the electrospinning process. (c) Si/TiO<sub>2</sub>/CNF obtained after carbonization.



**Fig. 2.** FESEM images of Si/CNF, TiO<sub>2</sub>/CNF, and Si/TiO<sub>2</sub>/CNF.

outstanding cycling stability.

To examine the nanostructural configuration, TEM analysis was carried out. Fig. 3 shows low-resolution (Fig. 3a–c) and high-resolution (Fig. 3d–f) TEM images of Si/CNF, TiO<sub>2</sub>/CNF, and Si/TiO<sub>2</sub>/CNF. Si/CNF (Fig. 3a and d) showed sparsely aggregated Si nanoparticles. Thus, the CNF matrix was not used efficiently for the capsulation of Si nanoparticles. Aggregated Si nanoparticles can easily break the CNF matrix during cycling. TiO<sub>2</sub>/CNF (Fig. 3b and e) showed high-dispersed TiO<sub>2</sub> nanoparticles in the CNF matrix, indicating that the TiO<sub>2</sub> nanoparticles with a high zeta

potential in DNF solution could utilize the CNF matrix. Interestingly, Si/TiO<sub>2</sub>/CNF (Fig. 3c and f) displayed the high-dispersed Si and TiO<sub>2</sub> nanoparticles in the CNF matrix without the aggregation of nanoparticles. Thus, the complexation of TiO<sub>2</sub> nanoparticles could assist the dispersion of Si nanoparticles.

To further investigate the distributions of Si and TiO<sub>2</sub> nanoparticles in the CNF matrix of Si/TiO<sub>2</sub>/CNF, TEM–EDS mapping was performed, as shown in Fig. 4. All atoms are uniformly dispersed along the nanofiber structure, which means that the Si and TiO<sub>2</sub> nanoparticles are consistently formed in the CNF matrix.

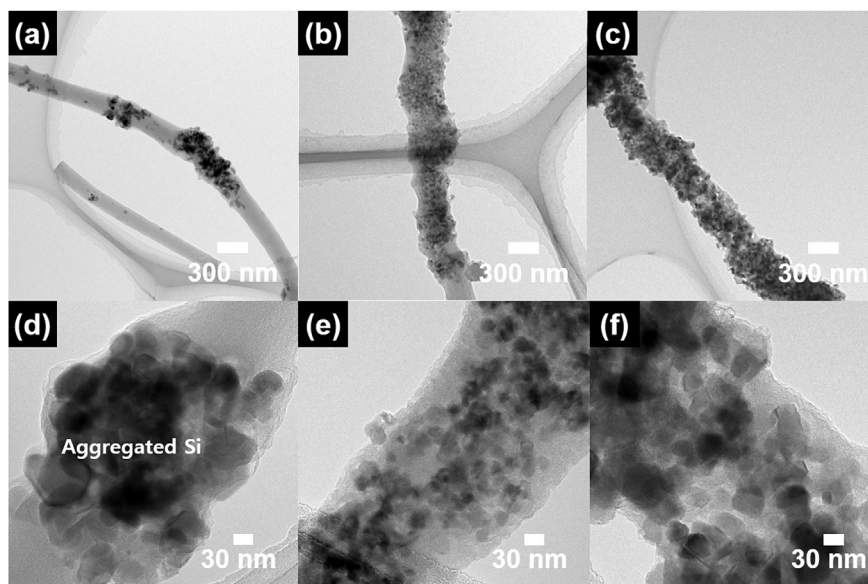


**Fig. 3.** Low-resolution (a–d) and high-resolution (e–h) TEM images of Si/CNF, TiO<sub>2</sub>/CNF, and Si/TiO<sub>2</sub>/CNF.

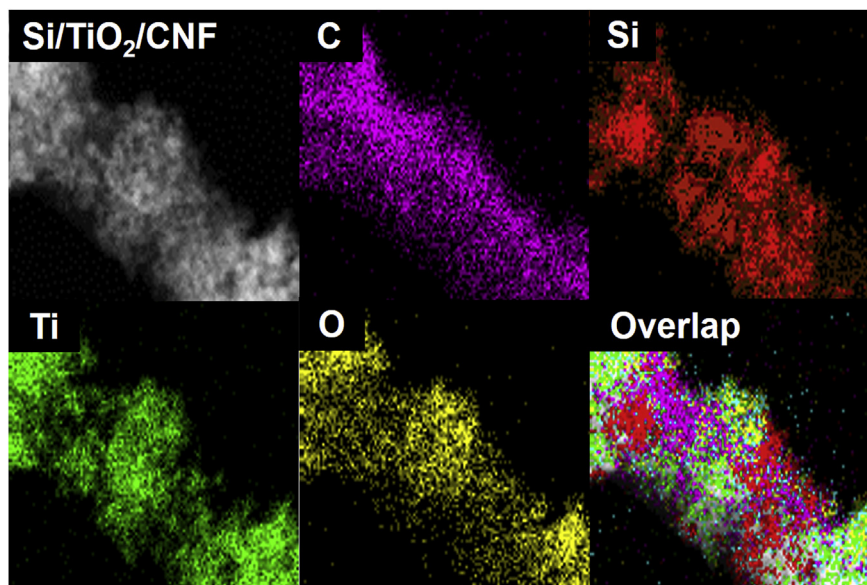


Fig. 4. TEM–EDS mapping data of Si/TiO<sub>2</sub>/CNF.

Based on the SEM, TEM, and TEM–EDS mapping results, a formation mechanism of Si/TiO<sub>2</sub>/CNF is schematically illustrated in Fig. 5. Interestingly, high-dispersed Si nanoparticles in the CNF matrix were successfully obtained, leading to the efficient accommodation of the volume change during cycling. These results can be explained in terms of two reasons. First, the high-dispersed TiO<sub>2</sub> nanoparticles in DMF solution could physically assist the dispersion of Si nanoparticles. Second, the small size of TiO<sub>2</sub> nanoparticles compared with Si nanoparticles enabled their complexation between the Si nanoparticles.

Fig. 6a shows XRD data used to explore the crystal structures. Si/CNF showed broad peaks around 25°, corresponding to the graphite layers (002) of CNF, and diffraction peaks at 28.6°, corresponding to the (111) plane of Si with a face-centered structure (JCPDS card No. 80-0018). The diffraction peaks of TiO<sub>2</sub>/CNF were divided into anatase and rutile phases. First, the anatase phase was observed at 25.3°, 37.8°, and 48.1°, corresponding to the (101), (004), and (200) planes, respectively. Second, the rutile phase was surveyed at 27.6°, 36.2°, and 54.6°, corresponding to the (110), (101), and (211) planes, respectively. Moreover, Si/TiO<sub>2</sub>/CNF indicated the presence of mixed phases consisting of Si and TiO<sub>2</sub>, implying the successful complexation with Si, TiO<sub>2</sub>, and CNF. In addition, the concentration

of nanoparticles in CNF was recognized by TGA measurements, as shown in Fig. 6b. Si/CNF exhibited weight losses of 72%, signifying the presence of Si nanoparticles in the CNFs. Additionally, the weight loss of Si/CNF successively increased with the increasing temperature, suggesting the formation of silicon oxidation [28,32,33]. TiO<sub>2</sub>/CNF exhibited a weight loss of 57% owing to the existence of TiO<sub>2</sub> nanoparticles in the CNF. Si/TiO<sub>2</sub>/CNF presented low weight losses of 45% compared to other samples, indicating that the decreased weight loss may be attributed to the complexation of TiO<sub>2</sub> nanoparticles in Si/CNF. The TGA outcomes are thus in good agreement with the TEM-mapping results.

To study the electrochemical behavior of electrodes, cycling tests were carried out using coin-type half cells in a voltage range of 0.05–3.00 V (vs. Li/Li<sup>+</sup>). For comparison, Si nanoparticles were prepared (referred to as only-Si). Fig. 7a shows the Coulombic efficiency during 100 cycles. All electrodes displayed the low Coulombic efficiency for the first cycle, owing to the direct formation of solid–electrolyte interface (SEI) layers on the surface [5,6]. SEI layers are usually constructed because of the reductive decomposition of electrolyte components on the electrode surface, leading to high initial irreversible reactions [5,6]. Nonetheless, the Si/TiO<sub>2</sub>/CNF electrode showed a higher Coulombic efficiency

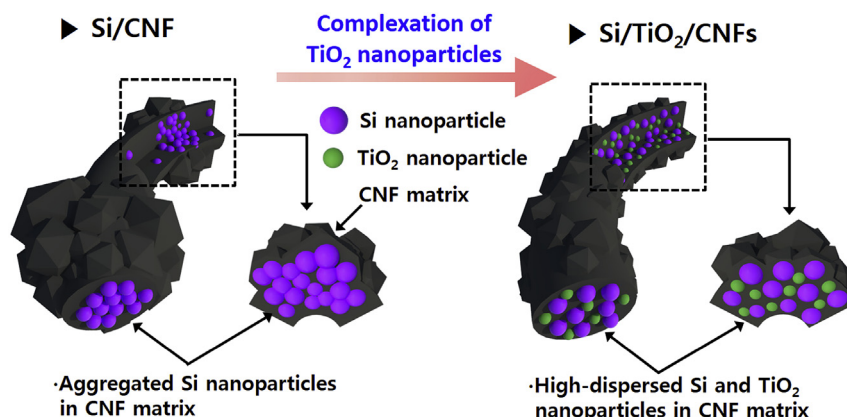


Fig. 5. Schematic illustration of the complexation of TiO<sub>2</sub> nanoparticles of Si/TiO<sub>2</sub>/CNF.

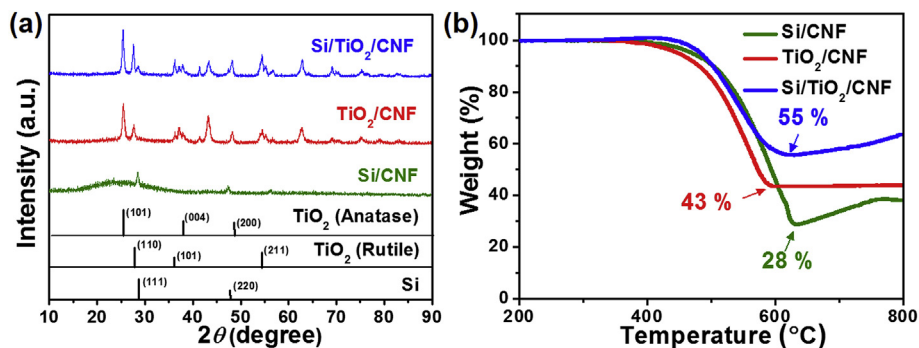


Fig. 6. (a) XRD patterns of Si/CNF, TiO<sub>2</sub>/CNF, and Si/TiO<sub>2</sub>/CNF. (b) TGA curves of Si/CNF, TiO<sub>2</sub>/CNF, and Si/TiO<sub>2</sub>/CNF from 200 to 800 °C at a heating rate of 10 °C min<sup>-1</sup> in air.

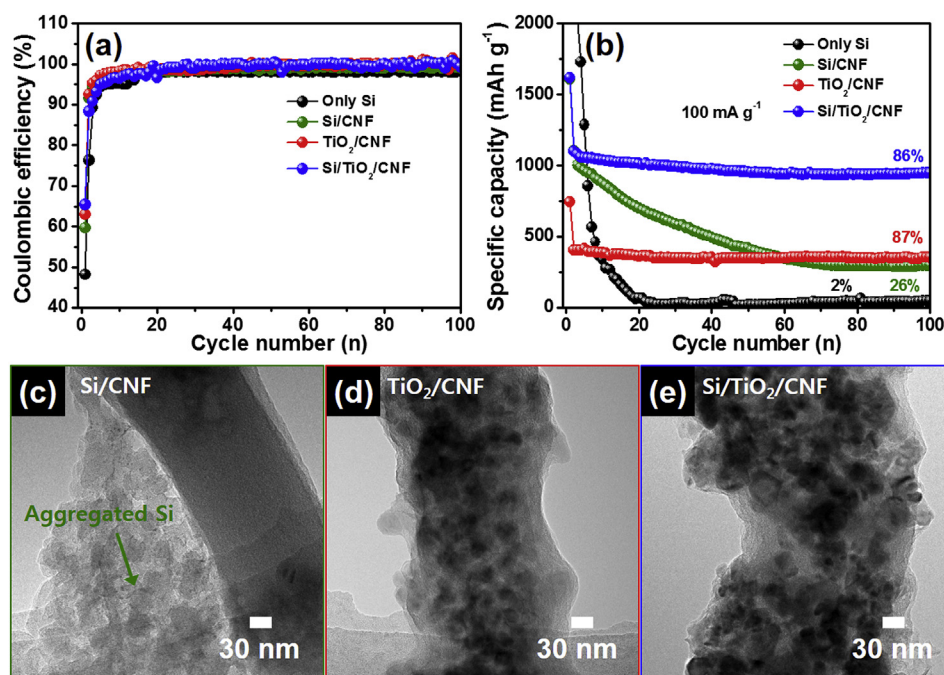
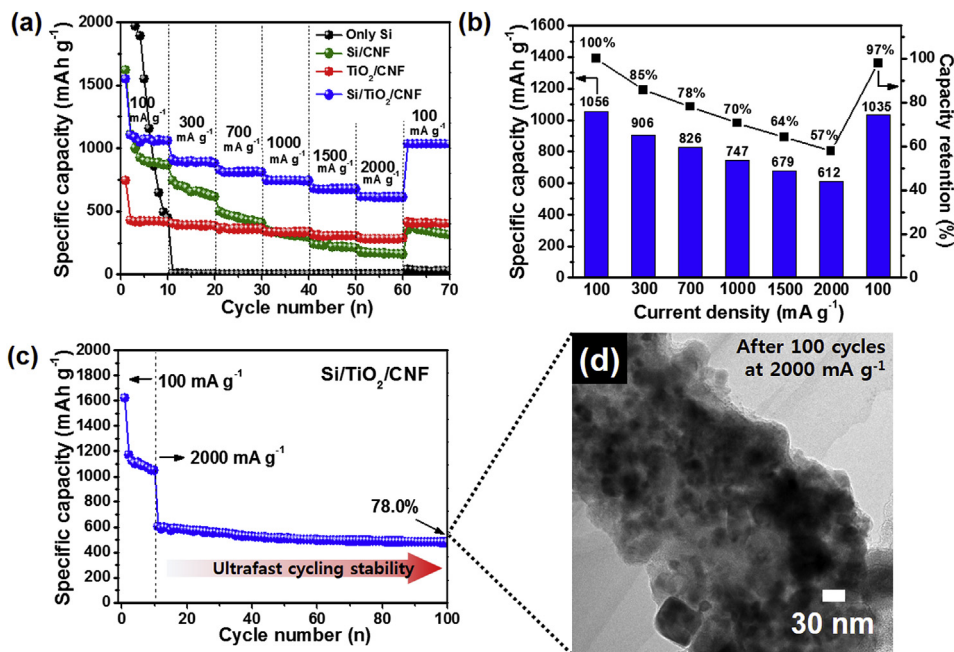


Fig. 7. (a) Coulombic efficiency and (b) Cycling stability of Si/CNF, TiO<sub>2</sub>/CNF, and Si/TiO<sub>2</sub>/CNF electrodes at current densities of 100 mA g<sup>-1</sup> up to 100 cycles. TEM images of (c) Si/CNF, (d) TiO<sub>2</sub>/CNF, and (e) Si/TiO<sub>2</sub>/CNF after 100 cycles.

(65.3%) than the only-Si (48.1%), Si/CNF (59.6%), and TiO<sub>2</sub>/CNF electrodes (62.9%). This reveals that the high-dispersed Si nanoparticles using a complexation of TiO<sub>2</sub> nanoparticles can play an important role for the improvement of Coulombic efficiency during the first cycles. Furthermore, the Coulombic efficiency of all electrodes reached nearly 100% after seven cycles, signifying high reversible reactions for LIBs. Fig. 7b indicates the cycling performance with the discharge capacity of only-Si, Si/CNF, TiO<sub>2</sub>/CNF, and Si/TiO<sub>2</sub>/CNF electrodes at a current density of 100 mA g<sup>-1</sup> up to 100 cycles. The only-Si electrode displayed a rapid specific capacity drop to 48 mA h g<sup>-1</sup> after 100 cycles. It is well known that Si can be dramatically expanded by approximately ~300% during the insertion/extraction of Li ions. Si/CNF electrode showed a poor cycling stability with a specific capacity of 297 mA h g<sup>-1</sup> after 100 cycles. This result indicates that Si/CNF suffers from a large volume change based on aggregated Si nanoparticles during insertion/extraction of Li ions. Thus, a complexation with TiO<sub>2</sub> nanoparticles is necessary to improve the dispersion of Si nanoparticles, leading to an effective accommodation of the volume change of Si nanoparticles. The TiO<sub>2</sub>/CNF electrode exhibited superb cycling stability with a specific

capacity of 353 mA h g<sup>-1</sup> after 100 cycles, owing to the small volume change of TiO<sub>2</sub>. Nevertheless, the low specific capacity of TiO<sub>2</sub>/CNF is attributed to low theoretical capacity of TiO<sub>2</sub>. For this reason, we suggested the Si/TiO<sub>2</sub>/CNF electrode to achieve a high specific capacity using Si nanoparticles and an excellent cycling stability using TiO<sub>2</sub> nanoparticles and a CNF matrix. Notably, the Si/TiO<sub>2</sub>/CNF electrode exhibited a splendid cycling stability with a high specific capacity of 947 mA h g<sup>-1</sup> after 100 cycles, which is higher than any previously reported values for Si/CNF composites, as listed in Table S1 [23–38]. Therefore, we suggest that the monitored outstanding cycling stability with a high specific capacity of Si/TiO<sub>2</sub>/CNF electrode may be primarily attributed to the unique composite structure. There are two causes based on the high-dispersed Si nanoparticles for the improved electrochemical performance: (1) effective accommodation of the volume change of Si nanoparticles relative to an enhanced cycling stability, (2) increased electroactive sites of Si nanoparticles related to a high specific capacity. Furthermore, the CV curves of the Si/TiO<sub>2</sub>/CNF electrode exhibited the typical electrochemical reactions of Si, TiO<sub>2</sub>, and carbon, as shown in Fig. S3. To further observe the detailed morphological and



**Fig. 8.** (a) High-rate performance of all electrodes at current densities of 100, 300, 700, 1000, 1500, 2000, and 100 mA g<sup>-1</sup>. (b) The detailed specific capacities and capacity retentions of Si/TiO<sub>2</sub>/CNF electrode with increasing current densities. (c) Ultrafast cycling stability of Si/TiO<sub>2</sub>/CNF electrode at 100 mA g<sup>-1</sup> and 2000 mA g<sup>-1</sup>. (d) TEM analysis of Si/TiO<sub>2</sub>/CNF electrode after 100 cycles at 2000 mA g<sup>-1</sup>.

structural changes of all electrodes after 100 cycles, TEM analysis has been performed using the decomposed coin-type half cells. The aggregated Si nanoparticles of Si/CNF (Fig. 7c) were separated from the CNF matrix, signifying the inefficient utilization of the CNF matrix. On the other hand, TiO<sub>2</sub>/CNF (Fig. 7d) still retained its original structure after 100 cycles, owing to the high dispersion and low volume change of the TiO<sub>2</sub> nanoparticles. Moreover, Si/TiO<sub>2</sub>/CNF (Fig. 7e) maintained its original structure after 100 cycles, indicating that unique composites of Si/TiO<sub>2</sub>/CNF could accommodate the volume change of Si nanoparticles based on high-dispersed Si nanoparticles in the CNF matrix.

With the growth of the LIB industry, high-rate performance and ultrafast cycling stability are important topics for the expansion of its application fields. Fig. 8a presents the high-rate performance of only-Si, Si/CNF, TiO<sub>2</sub>/CNF, and Si/TiO<sub>2</sub>/CNF electrodes at different current densities of 100, 300, 700, 1000, 1500, 2000, and 100 mA g<sup>-1</sup>. The specific capacities of all electrodes reduced with increasing current densities, owing to the reduced diffusion time of Li ions during cycling. Only-Si electrodes showed low specific capacities at high-rate current densities, similar to that at the low-rate current density of 100 mA g<sup>-1</sup>. Si/CNF showed a poor high-rate performance of 178 mA h g<sup>-1</sup> at 2000 mA g<sup>-1</sup> because of the longer diffusion path of Li ions, owing to aggregated Si nanoparticles. On the other hand, TiO<sub>2</sub>/CNF exhibited a good high-rate performance of 285 mA h g<sup>-1</sup> at 2000 mA g<sup>-1</sup>, owing to a shorter diffusion path of Li ions related to high-dispersed TiO<sub>2</sub> nanoparticles. Remarkably, the Si/TiO<sub>2</sub>/CNF electrode manifested a notable high-rate performance of 612 mA h g<sup>-1</sup> at 2000 mA g<sup>-1</sup>. The Si/TiO<sub>2</sub>/CNF electrode showed the highest high-rate performance, greater than previously reported values for Si/CNF composites, as shown in Fig. S4 [29,31–33,38].

To further verify the high-rate performance of the Si/TiO<sub>2</sub>/CNF electrode, the specific capacities and the capacity retentions with increasing current densities have been listed (Fig. 8b). The Si/TiO<sub>2</sub>/CNF electrode displayed an excellent capacity retention of 97.9% when the current density recovered to 100 mA g<sup>-1</sup> after high-rate tests. The enhanced high-rate performance of Si/TiO<sub>2</sub>/CNF is

attributed to the shorter diffusion path of Li ions based on the high-dispersed Si nanoparticles in the CNF matrix. The high-rate performance results related to the Li ion diffusion were successfully confirmed by EIS measurements, as shown in Fig. S5. The high-dispersed Si nanoparticles could reduce the Warburg impedance, leading to enhanced high-rate performance in LIBs. In addition, the ultrafast cycling stability of Si/TiO<sub>2</sub>/CNF electrode was measured at a high current density of 2000 mA g<sup>-1</sup>, as shown in Fig. 8c. The Si/TiO<sub>2</sub>/CNF electrode indicated the superb ultrafast cycling stability with a specific capacity of 478 mA h g<sup>-1</sup> after 100 cycles as well as a good capacity retention of 78.0%. To demonstrate the structural stability of Si/TiO<sub>2</sub>/CNF after an ultrafast cycling test, TEM analysis was performed using decomposed coin-type cells, as shown in Fig. 8d. As expected, the CNF matrix was still attached with Si and

### Unique architecture for ultrafast lithium storage

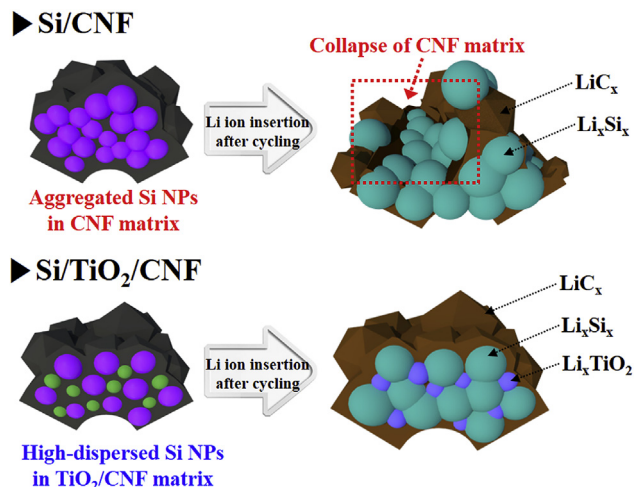


**Fig. 9.** Schematic of Si/TiO<sub>2</sub>/CNF with three main influences for high-performance LIBs.

TiO<sub>2</sub> nanoparticles without any serious structural collapse. The stable electrochemical reactions of the Si/TiO<sub>2</sub>/CNF electrode during the ultrafast cycling are ascribed to the shorter diffusion path of Li ions based on high-dispersed Si nanoparticles in the CNF matrix, which could facilitate the fast movement of Li ions.

We clearly demonstrated that the enhanced electrochemical properties of the Si/TiO<sub>2</sub>/CNF electrode can be clarified as follows (Fig. 9): (1) complexation with TiO<sub>2</sub> nanoparticles improved the dispersion of Si nanoparticles, provided an enhanced cycling stability with high capacity owing to effective accommodation of the volume change of Si nanoparticles as well as increased electroactive sites of Si nanoparticles, (2) high-dispersed Si nanoparticles could also reduce the diffusion path of Li ions, leading to outstanding high-rate performance.

#### 4. Conclusions

We synthesized Si/TiO<sub>2</sub>/CNF as an anode material for LIBs using electrospinning and the carbonization. To improve the dispersion of Si nanoparticles, complexation of TiO<sub>2</sub> nanoparticles was performed in the CNF matrix. Si/TiO<sub>2</sub>/CNF formed a unique composite consisting of high-dispersed Si and TiO<sub>2</sub> nanoparticles in the CNF matrix. The Si/TiO<sub>2</sub>/CNF electrode showed improved LIB performance, including excellent cycling stability with a high specific capacity (947 mA h g<sup>-1</sup> at 100 mA g<sup>-1</sup> after 100 cycles), and superb high-rate performance (612 mA h g<sup>-1</sup> at 2000 mA g<sup>-1</sup>). Furthermore, the Si/TiO<sub>2</sub>/CNF electrode displayed a striking ultrafast cycling stability (478 mA h g<sup>-1</sup> at 2000 mA g<sup>-1</sup> after 100 cycles) without any serious structural collapse. The improved LIB performance can be described in terms of two main influences. First, the outstanding cycling stability with high capacity is ascribed to the high-dispersed Si nanoparticles based on efficient accommodation of the volume change of Si nanoparticles, as well as increased electroactive sites of Si nanoparticles. Second, the excellent ultrafast cycling stability is attributed to the shorter diffusion path of Li ions. We believe that this unique composite has exceptional potential as an anode material in LIBs.

#### Acknowledgments

This research was supported by Basic Science Research Program through the National Research Foundation of Korea (NRF) funded by the Ministry of Science, ICT and Future Planning (NRF-2015R1A1A1A05001252).

#### Appendix A. Supplementary data

Supplementary data related to this article can be found at <http://dx.doi.org/10.1016/j.jallcom.2017.03.273>.

#### References

- [1] M. Armand, J.M. Tarascon, *Nature* 451 (2008) 652–657.
- [2] P.G. Bruce, B. Scrosati, J.M. Tarascon, *Nature* 47 (2008) 2930–2946.

- [3] C. Liang, M. Gao, H. Pan, Y. Liu, M. Yan, *J. Alloys Compd.* 573 (2013) 246–256.
- [4] G.H. An, D.Y. Lee, H.J. Ahn, *ACS Appl. Mater. Interfaces* 8 (2016) 19466–19474.
- [5] G.H. An, D.Y. Lee, Y.J. Lee, H.J. Ahn, *ACS Appl. Mater. Interfaces* 8 (2016) 30264–30270.
- [6] G.H. An, J.I. Sohn, H.J. Ahn, *J. Mater. Chem. A* 4 (2016) 2049–2054.
- [7] L. Ji, Z. Lin, M. Alcoutlabi, X. Zhang, *Energy Environ. Sci.* 4 (2011) 2682–2699.
- [8] V. Etacheri, R. Marom, R. Elazari, G. Salitra, D. Aurbach, *Energy Environ. Sci.* 4 (2011) 3243–3262.
- [9] H. Li, Z. Wang, L. Chen, X. Huang, *Adv. Mater.* 21 (2009) 4593–4607.
- [10] Z. Wu, B. Li, Y. Xue, J. Li, Y. Zhang, F. Gao, *J. Mater. Chem. A* 3 (2015) 19445–19454.
- [11] S. Yu, J.-W. Jung, I.-D. Kim, *Nanoscale* 7 (2015) 11945–11950.
- [12] J. Jiang, C. Wang, W. Liabed, Q. Yang, *J. Mater. Chem. A* 3 (2015) 23345–23351.
- [13] J. Gu, Y. Zeng, X. Feng, X. Wu, C. Zeng, M. Li, *J. Alloys Compd.* 662 (2016) 185–192.
- [14] S.H. Baek, J.S. Park, Y.M. Jeong, J.H. Kim, *J. Alloys Compd.* 660 (2016) 387–391.
- [15] J. Wu, Z. Zhu, H. Zhang, H. Fu, H. Li, A. Wang, H. Zhang, Z. Hu, *J. Alloys Compd.* 596 (2014) 86–91.
- [16] B.D. Polat, O. Keles, *J. Alloys Compd.* 677 (2016) 228–236.
- [17] J. Li, J. Wang, J. Yang, X. Ma, S. Lu, *J. Alloys Compd.* 688 (2016) 1072–1079.
- [18] J.P. Yen, C.C. Chang, Y.R. Lin, S.T. Shen, J.L. Hong, *J. Alloys Compd.* 598 (2014) 184–190.
- [19] R. Zhou, R. Fan, Z. Tian, Y. Zhou, H. Guo, L. Kou, D. Zhang, *J. Alloys Compd.* 658 (2016) 91–97.
- [20] A.L. Silva, M.M. Correa, G.C.D. Oliveira, P.P.F. Rodriguez, C.A.R. Costa, F.S. Semaan, E.A. Ponzio, *J. Alloys Compd.* 691 (2017) 200–229.
- [21] R. Zhou, H. Guo, Y. Yang, Z. Wang, X. Li, Y. Zhou, *J. Alloys Compd.* 689 (2016) 130–137.
- [22] Q. Wu, T. Tran, W. Lu, J. Wu, *J. Power Sources* 258 (2014) 39–45.
- [23] B.S. Lee, S.B. Son, K.M. Park, J.H. Seo, S.H. Lee, I.S. Choi, K.H. Oh, W.R. Yu, *J. Power Sources* 206 (2012) 267–273.
- [24] K. Fu, Y. Lu, M. Dirican, C. Chen, M. Yanilmaz, Q. Shi, P.D. Bradford, X. Zhang, *Nanoscale* 6 (2014) 7489–7495.
- [25] N.T. Hieu, J. Suk, D.W. Kim, O.H. Chung, J.S. Park, Y. Kang, *Synth. Met.* 198 (2014) 36–40.
- [26] Y. Li, B. Guo, L. Ji, Z. Lin, G. Xu, Y. Liang, S. Zhang, O. Toprakci, Y. Hu, M. Alcoutlabi, X. Zhang, *Carbon* 51 (2013) 185–194.
- [27] L. Xue, K. Fu, Y. Li, G. Xu, Y. Lu, S. Zhang, O. Toprakci, X. Zhang, *Nano Energy* 2 (2013) 361–367.
- [28] L. Ji, X. Zhang, *Energy Environ. Sci.* 3 (2010) 124–129.
- [29] M. Dirican, O. Yildiz, Y. Lu, X. Fang, H. Jiang, H. Kizil, X. Zhang, *Electrochim. Acta* 169 (2015) 52–60.
- [30] Y. Li, Y. Sun, G. Xu, Y. Lu, S. Zhang, L. Xue, J.S. Jur, X. Zhang, *J. Mater. Chem. A* 2 (2014) 11417–11425.
- [31] Y. Liu, K. Huang, Y. Fan, Q. Zhang, F. Sun, T. Gao, Z. Wang, *J. Zhong. Electrochim. Acta* 102 (2013) 246–251.
- [32] M.S. Wang, W.L. Song, J. Wang, L.Z. Fan, *Carbon* 82 (2015) 337–345.
- [33] Z.L. Xu, B. Zhang, J.K. Kim, *Nano Energy* 6 (2014) 27–35.
- [34] X. Fan, L. Zou, Y.P. Zheng, F.Y. Kang, W.C. Shen, *Electrochem. Solid-State Lett.* 12 (2009) A199–A201.
- [35] B.S. Lee, S.B. Son, J.H. Seo, K.M. Park, G. Lee, S.H. Lee, K.H. Oh, J.P. Ahn, W.R. Yu, *Nanoscale* 5 (2013) 4790–4796.
- [36] B.S. Lee, H.S. Yang, H. Jung, S.Y. Jeon, C. Jung, S.W. Kim, J. Bae, C.L. Choong, J. Im, U.I. Chung, J.J. Park, W.R. Yu, *Nanoscale* 6 (2014) 5989–5998.
- [37] J. Shin, K. Park, W.H. Ryu, J.W. Jung, I.D. Kim, *Nanoscale* 6 (2014) 12718–12726.
- [38] Y. Chen, Y. Hu, J. Shao, Z. Shen, R. Chen, X. Zhang, X. He, Y. Song, X. Xing, *J. Power Sources* 298 (2015) 130–137.
- [39] B. Zhao, S. Jiang, C. Su, R. Cai, R. Ran, M.O. Tade, Z. Shao, *J. Mater. Chem. A* 1 (2013) 12310–12320.
- [40] X. Li, Y. Chen, L. Zhou, Y.W. Mai, H. Huang, *J. Mater. Chem. A* 2 (2014) 3875–3880.
- [41] Z. Yang, G. Du, Q. Meng, Z. Guo, X. Yu, Z. Chen, T. Guo, R. Zeng, *J. Mater. Chem.* 22 (2012) 5848–5854.
- [42] G.H. An, H.J. Ahn, *J. Power Sources* 272 (2014) 828–836.
- [43] G.H. An, S.J. Kim, K.W. Park, H.J. Ahn, *ECS Solid State Lett.* 3 (2014) M21–M23.
- [44] G.H. An, E.H. Lee, H.J. Ahn, *Phys. Chem. Chem. Phys.* 18 (2016) 14859–14866.
- [45] Y. Wang, D. Li, Y. Liu, J. Zhang, *Electrochim. Acta* 203 (2016) 84–90.
- [46] G. Hou, B. Cheng, Y. Cao, M. Yao, B. Li, C. Zhang, Q. Weng, X. Wang, Y. Bando, D. Golberg, F. Yuan, *Nano Energy* 24 (2016) 111–120.